

Entropy-induced smectic phases in rod–coil copolymers

Dominik Düchs¹ and D E Sullivan²

¹ Fakultät für Physik, Universität Bielefeld, Universitätsstrasse 25, 33615 Bielefeld, Germany

² Department of Physics and Guelph-Waterloo Physics Institute, University of Guelph, Guelph, Ontario, Canada N1G 2W1

Received 5 June 2002

Published 8 November 2002

Online at stacks.iop.org/JPhysCM/14/12189

Abstract

We present a self-consistent field theory (SCFT) for dilute solutions of semiflexible (wormlike) diblock copolymers, each consisting of a rigid and a flexible part. The segments of the polymers are otherwise identical, in particular with regard to their interactions, which are taken to be of an Onsager excluded-volume type. The theory is developed in a general three-dimensional form, as well as in a simpler one-dimensional version. Using the latter, we demonstrate that the theory predicts the formation of a partial-bilayer smectic-A phase in this system, as shown by profiles of the local density and orientational distribution functions. The phase diagram of the system, which includes the isotropic and nematic phases, is obtained in terms of the mean density and rigid-rod fraction of each molecule. The nematic–smectic transition is found to be second order. Since the smectic phase is induced solely by the difference in the rigidities, the onset of smectic ordering is shown to be an entropic effect and therefore does not have to rely on additional Flory–Huggins-type repulsive interactions between unlike chain segments. These findings are compared with other recent SCFT studies of similar copolymer models and with computer simulations of several molecular models.

1. Introduction

Liquid crystals, being of major importance both on fundamental grounds and for industrial applications, have long been of interest to researchers [1, 2]. Another class of materials of considerable interest are melts of block copolymers, which have been shown in recent decades to exhibit a multitude of phases of varying complexity [3]. This paper will be concerned with liquid-crystalline copolymers, i.e. copolymers which exhibit phases commonly associated with liquid crystals.

For the study of nonuniform polymer melts, a particular type of mean-field density-functional approach traditionally known as self-consistent field theory (SCFT) has proven

to be a very powerful tool [4–8]. Aside from obvious determinants like the composition of the melt being studied, the models considered by SCFT approaches differ mainly in two regards: the flexibility of the polymer chain and the interactions between chain segments. Most commonly, polymers have been modelled as perfectly flexible Gaussian chains, which assumes that there is no energy penalty for local bending. Alternatively, the ‘wormlike’ chain model [9, 10] does introduce such a bending penalty and is thus the appropriate model for semiflexible polymers. Concerning the interactions, most previous investigators have invoked Flory–Huggins-type repulsive interactions between unlike chain segments in order to induce microphase separation and hence the formation of various mesoscopic phases [8, 11, 12].

The aim of the present paper is to develop a modified SCFT suited to examining the formation of liquid-crystalline phases in athermal solutions of diblock copolymers, each consisting of a rigid (‘rod’) and a flexible (‘coil’) part. Both parts are modelled as wormlike chains, but are characterized by different rigidities. For the interactions between any two chain segments, in this work we do not distinguish between the two parts, i.e. we assume that the same type of interaction applies to any pair of chain segments. We take this interaction to be the limit of the Onsager excluded-volume interaction for thin rods, which favours local alignment of the chains. In the case of homogeneous chains, characterized throughout by the same rigidity, the present model reduces to that applied by Chen *et al* [13, 14] to the study of nematic ordering and the isotropic–nematic interface of semiflexible polymers. As is well known [13, 15], the Onsager model is based on a second-virial approximation to the free energy, and hence is strictly valid only for dilute polymer solutions. Here we show that the generalized model with different rigidities for two parts of a polymer is able to account for the formation of lamellar smectic-A phases. With this minimal model, the only possible sources for the formation of such phases are entropic effects. Recently, both smectic monolayer and bilayer phases (traditionally denoted A_1 and A_2) have been found in a SCFT-based approach which includes Flory–Huggins interactions and treats the rigid sections of the polymers as perfectly rigid and perfectly aligned in the same orientation [16, 17]. In contrast, here we find only one type of smectic-A phase, which would most accurately be classified as a partial bilayer phase (denoted A_d). In addition, as in [13, 14], our model accounts for the disordered isotropic phase.

Liquids of fairly *short* rod–coil molecules have been examined recently by computer simulations [18–23]. Generally, these computer studies have shown that the addition of flexible segments to otherwise rigid molecules stabilizes the smectic-A phase with respect to the nematic phase, consistent with experimental results for thermotropic non-polymeric liquid crystals [2]. This behaviour is also shown by the present model, although, in contrast to some studies [19, 20, 22], we do not find that the nematic phase is entirely suppressed with respect to the isotropic and smectic phases. Our finding that the only stable smectic-A of the present model is the partial bilayer A_d phase is in agreement with a density-functional treatment by Holyst [24] of rigid ‘nail-shaped’ molecules and, somewhat more tentatively, with Monte Carlo studies by Mazars *et al* [20] of a rod–coil model.

Experimental studies by Chen *et al* [25] demonstrated both monolayer and bilayer smectic ordering in rod–coil diblock copolymers consisting of a highly rigid polyhexyl–isocyanate block joined to a flexible polystyrene coil. However, these results were complicated by the simultaneous occurrence of tilted (or smectic-C) ordering and crystallization of the rigid blocks. These two effects are not considered here, but will be examined in future work.

This paper is organized as follows. In section 2, a detailed description of the theory is given. In section 3, numerical results are presented, showing the local density and orientational order-parameter profiles in the smectic phase as well as the phase diagram of the model in terms of mean density and rod fraction. We conclude with a summary and discussion in section 4.

2. Theory

2.1. General three-dimensional theory

We consider a monodisperse solution of n rod-coil diblock copolymers in a structureless solvent, occupying a total volume V . Each copolymer is characterized by a total contour length L , polymerization index N and fixed segment length a such that $L = Na$. A fraction f of the total contour length of each copolymer is occupied by relatively rigid (rod) segments, and the remaining fraction by more flexible (coil) segments. The average number density n/V of copolymers is denoted by ρ . In accordance with the wormlike chain model for semiflexible chains [9–14], which is applied here to both sections of the chains, polymers will be treated as space curves $\mathbf{r}_i(t)$ characterized by dimensionless unit tangent vectors $\mathbf{u}_i(t)$. Hence, microscopic contour-averaged density operators may be defined as

$$\begin{aligned}\hat{\phi}_{rigid}(\mathbf{r}, \mathbf{u}) &= \frac{1}{\rho} \sum_{i=1}^n \int_0^f dt_i \delta(\mathbf{r} - \mathbf{r}_i(t_i)) \delta(\mathbf{u} - \mathbf{u}_i(t_i)), \\ \hat{\phi}_{flex}(\mathbf{r}, \mathbf{u}) &= \frac{1}{\rho} \sum_{i=1}^n \int_f^1 dt_i \delta(\mathbf{r} - \mathbf{r}_i(t_i)) \delta(\mathbf{u} - \mathbf{u}_i(t_i)),\end{aligned}\quad (1)$$

which satisfy the normalization conditions

$$\int d\mathbf{r} d\mathbf{u} \hat{\phi}_{rigid}(\mathbf{r}, \mathbf{u}) = fV, \quad \int d\mathbf{r} d\mathbf{u} \hat{\phi}_{flex}(\mathbf{r}, \mathbf{u}) = (1-f)V. \quad (2)$$

Since these partial densities are only determined *a posteriori* and otherwise do not enter the calculations, we shall instead use the total density:

$$\hat{\phi}(\mathbf{r}, \mathbf{u}) = \hat{\phi}_{rigid}(\mathbf{r}, \mathbf{u}) + \hat{\phi}_{flex}(\mathbf{r}, \mathbf{u}). \quad (3)$$

The interaction potential between any two segments, i.e. rod-rod, rod-coil or coil-coil, is taken to be the Onsager excluded-volume interaction, which in the limit of very thin polymers ($L, a \gg$ diameter D) reduces to [14]

$$v(\mathbf{r}_1, \mathbf{u}_1; \mathbf{r}_2, \mathbf{u}_2) = L^2 D \delta(\mathbf{r}_1 - \mathbf{r}_2) |\mathbf{u}_1 \times \mathbf{u}_2|. \quad (4)$$

This interaction is minimized when contacting segments are parallel, i.e. $|\mathbf{u}_1 \times \mathbf{u}_2| = 0$. Since equation (4) describes the effects of hard-core repulsion between chain segments, at least at the level of a second-virial approximation [15], here we shall not impose an additional incompressibility constraint to account for such effects, as is commonly done in the theory of dense copolymer melts [7, 8].

The partition function in the canonical ensemble has the form

$$Z = \int \mathcal{D}_n\{\cdot\} \exp\left(-\rho C \int d\mathbf{r} \int d\mathbf{u} \int d\mathbf{u}' \hat{\phi}(\mathbf{r}, \mathbf{u}) \hat{\phi}(\mathbf{r}, \mathbf{u}') |\mathbf{u} \times \mathbf{u}'|\right), \quad (5)$$

where

$$C = L^2 D \rho \quad (6)$$

is proportional to the average polymer number density ρ . In equation (5),

$$\int \mathcal{D}_n\{\cdot\} \equiv \frac{1}{n!} \prod_{i=1}^n \int \mathcal{D}\{\mathbf{r}_i, \mathbf{u}_i\} \mathcal{P}\{\mathbf{r}_i, \mathbf{u}_i[0, 1]\}, \quad (7)$$

where

$$\begin{aligned}\mathcal{P}\{\mathbf{r}_i, \mathbf{u}_i[s_1, s_2]\} &\propto \prod_{t=s_1}^{s_2} \delta[\mathbf{u}_i(t)^2 - 1] \delta\left[\mathbf{r}_i(t) - \mathbf{r}_i(s_1) - L \int_{s_1}^t ds \mathbf{u}_i(s)\right] \\ &\times \exp\left[-\frac{1}{2N} \int_{s_1}^{s_2} dt' \kappa(t') \left|\frac{d\mathbf{u}_i}{dt'}\right|^2\right]\end{aligned}\quad (8)$$

is the statistical weight of a given path and $\kappa(t)$ is a dimensionless bending modulus. According to the model considered here

$$\kappa(t) = \begin{cases} \kappa_{rigid}, & 0 \leq t < f \\ \kappa_{flex}, & f < t \leq 1. \end{cases} \quad (9)$$

As is a standard procedure in SCFTs, we now multiply the partition function by $1 = \int \mathcal{D}\{\phi(\mathbf{r}, \mathbf{u})\} \delta(\phi(\mathbf{r}, \mathbf{u}) - \hat{\phi}(\mathbf{r}, \mathbf{u}))$, which allows us to replace the operator $\hat{\phi}$ with the function ϕ . Then, using the exponential representation of the delta function, the partition function can be rewritten as $Z \propto \int \mathcal{D}\{W\} \int \mathcal{D}\{\phi\} \exp(-\mathcal{F}[W, \phi])$ with

$$\mathcal{F} = \rho \left[C \int d\mathbf{r} \int d\mathbf{u} \int d\mathbf{u}' \phi(\mathbf{r}, \mathbf{u}) \phi(\mathbf{r}, \mathbf{u}') |\mathbf{u} \times \mathbf{u}'| - \int d\mathbf{r} \int d\mathbf{u} W(\mathbf{r}, \mathbf{u}) \phi(\mathbf{r}, \mathbf{u}) \right] - \ln \left(\frac{Q^n}{n!} \right), \quad (10)$$

where

$$Q = \int \mathcal{D}_1\{\cdot\} \exp \left(- \int_0^1 dt W(\mathbf{r}(t), \mathbf{u}(t)) \right) \quad (11)$$

is the single-chain partition function. The function $W(\mathbf{r}, \mathbf{u})$ is identified with the potential energy, or field, generated by all polymers in the system as seen by a ‘test’ polymer.

Taking the saddle point of the free energy (10) with respect to $\phi(\mathbf{r}, \mathbf{u})$ and $W(\mathbf{r}, \mathbf{u})$, we obtain the mean-field equations:

$$W(\mathbf{r}, \mathbf{u}) = 2C \int d\mathbf{u}' \phi(\mathbf{r}, \mathbf{u}') |\mathbf{u} \times \mathbf{u}'|, \quad (12a)$$

$$\phi(\mathbf{r}, \mathbf{u}) = - \frac{V}{Q} \frac{\delta Q}{\delta W(\mathbf{r}, \mathbf{u})}. \quad (12b)$$

In this approximation, the function $\phi(\mathbf{r}, \mathbf{u})$ equals the statistical average $\langle \hat{\phi}(\mathbf{r}, \mathbf{u}) \rangle$ of the microscopic density. In order to solve these equations for the density, we need to express $Q[W]$ in terms of the end-segment distribution function defined by

$$q(\mathbf{r}, \mathbf{u}, t) = \int \mathcal{D}\{r_i, u_i\} \mathcal{P}\{r_i, u_i; [0, t]\} \delta(\mathbf{r} - \mathbf{r}_i(t)) \delta(\mathbf{u} - \mathbf{u}_i(t)) \times \exp \left[- \int_0^t ds W(\mathbf{r}_i(s), \mathbf{u}_i(s)) \right]. \quad (13)$$

The function $q^\dagger(\mathbf{r}, \mathbf{u}, t)$ is defined as the end-segment distribution function starting from the opposite end of the polymer. Hence

$$Q = \int d\mathbf{u} \int d\mathbf{r} q(\mathbf{r}, \mathbf{u}, t) q^\dagger(\mathbf{r}, \mathbf{u}, t), \quad (14)$$

where the contour variable t is arbitrary. With the above definitions of Q , q and q^\dagger , equation (12b) yields for the local density:

$$\phi(\mathbf{r}, \mathbf{u}) = \frac{V}{Q} \int_0^1 dt q(\mathbf{r}, \mathbf{u}, t) q^\dagger(\mathbf{r}, \mathbf{u}, t). \quad (15)$$

The average rigid and flexible densities, $\phi_{rigid}(\mathbf{r}, \mathbf{u})$ and $\phi_{flex}(\mathbf{r}, \mathbf{u})$, are given by expressions analogous to (15) on replacing the limits of integration over t as in equation (1). The end-segment distribution functions, or propagators, satisfy diffusion-like equations:

$$\begin{aligned} \frac{\partial}{\partial t} q(\mathbf{r}, \mathbf{u}, t) &= \left[-L\mathbf{u} \cdot \nabla_{\mathbf{r}} + \frac{1}{2\xi(t)} \nabla_{\mathbf{u}}^2 - W(\mathbf{r}, \mathbf{u}) \right] q(\mathbf{r}, \mathbf{u}, t), \\ \frac{\partial}{\partial t} q^\dagger(\mathbf{r}, \mathbf{u}, t) &= \left[-L\mathbf{u} \cdot \nabla_{\mathbf{r}} - \frac{1}{2\xi(t)} \nabla_{\mathbf{u}}^2 + W(\mathbf{r}, \mathbf{u}) \right] q^\dagger(\mathbf{r}, \mathbf{u}, t), \end{aligned} \quad (16)$$

with initial conditions $q(\mathbf{r}, \mathbf{u}, 0) = 1$ and $q^\dagger(\mathbf{r}, \mathbf{u}, 1) = 1$. Here we have defined the rigidity parameter $\xi(t) \equiv \kappa(t)/N$, depending on the chain contour variable t : $\xi(t)$ equals the persistence length of the corresponding chain section in units of the total contour length L [11]. This is where the difference between the rigid and flexible parts of the copolymer is accounted for.

To proceed with further analysis of the mean-field equations, we represent the orientational (\mathbf{u}) dependencies of the functions ϕ , W , q and q^\dagger using spherical-harmonic series:

$$\begin{aligned}\phi(\mathbf{r}, \mathbf{u}) &= \sum_{l,m} \phi_{lm}(\mathbf{r}) Y_{l,m}(\mathbf{u}), & W(\mathbf{r}, \mathbf{u}) &= \sum_{l,m} W_{lm}(\mathbf{r}) Y_{l,m}(\mathbf{u}), \\ q(\mathbf{r}, \mathbf{u}, t) &= \sum_{l,m} q_{lm}(\mathbf{r}, t) Y_{l,m}(\mathbf{u}), & q^\dagger(\mathbf{r}, \mathbf{u}, t) &= \sum_{l,m} q_{lm}^\dagger(\mathbf{r}, t) Y_{l,m}(\mathbf{u}).\end{aligned}\quad (17)$$

Since these are all real functions, the expansion coefficients must obey the following conditions:

$$\phi_{l,m}(\mathbf{r}) = \phi_{l,-m}^*(\mathbf{r})(-1)^m \quad (18)$$

etc. Next, we expand the kernel $|\mathbf{u} \times \mathbf{u}'|$ by use of the addition theorem for spherical harmonics [14]:

$$|\mathbf{u} \times \mathbf{u}'| = \sum_{l,m} \frac{4\pi}{2l+1} d_l Y_{l,m}(\mathbf{u}) Y_{l,m}^*(\mathbf{u}') \quad (19)$$

with

$$\begin{aligned}d_l &= 0, & l \text{ odd}, & & d_0 &= \frac{\pi}{4}, \\ d_{2k} &= -\frac{\pi(4k+1)(2k)!(2k-2)!}{2^{4k+1}(k-1)!k!k!(k+1)!}, & k &= 1, 2, 3, \dots\end{aligned}\quad (20)$$

Inserting these formulae into the free energy (10), the latter can be expressed as

$$\mathcal{F} = \rho \sum_{l,m} \int d\mathbf{r} \left[\frac{4\pi C}{2l+1} d_l |\phi_{l,m}(\mathbf{r})|^2 - \text{Re}(W_{l,m}(\mathbf{r}) \phi_{l,m}^*(\mathbf{r})) \right] - \ln \frac{Q^n}{n!}, \quad (21)$$

where ‘Re’ denotes the real part. The mean-field equations (12a) and (15) are now

$$W_{l,m}(\mathbf{r}) = \frac{8\pi}{2l+1} d_l C \phi_{l,m}(\mathbf{r}), \quad (22)$$

$$\begin{aligned}\phi_{l,m}(\mathbf{r}) &= \frac{V}{Q} \int_0^1 dt \sum_{l',m'} \sum_{l'',m''} q_{l',m'}^\dagger(\mathbf{r}, t) q_{l'',m''}(\mathbf{r}, t) \int d\mathbf{u} Y_{l',m'}(\mathbf{u}) Y_{l'',m''}(\mathbf{u}) Y_{l,m}^*(\mathbf{u}) \\ &= \frac{V}{Q} \int_0^1 dt \sum_{l',m'} \sum_{l'',m''} q_{l',m'}^\dagger(\mathbf{r}, t) q_{l'',m''}(\mathbf{r}, t) \sqrt{\frac{(2l''+1)(2l'+1)}{4\pi(2l+1)}} \\ &\quad \times C_{0,0,0}^{l'',l',l} C_{m'',m',m}^{l'',l',l},\end{aligned}\quad (23)$$

with

$$Q = \sum_{l,m} \int d\mathbf{r} q_{l,m}(\mathbf{r}, t) q_{l,-m}^\dagger(\mathbf{r}, t) (-1)^m. \quad (24)$$

The $C_{m'',m',m}^{l'',l',l}$ are Clebsch–Gordan coefficients, and we have used a result for the integral of three spherical harmonics [26]. The corresponding projections $\phi_{rigid,l,m}$ and $\phi_{flex,l,m}$ are obtained

likewise by changing the limits of the line integral in equation (23). In terms of the projections $q_{l,m}(\mathbf{r}, t)$, the diffusion-like equation (16) yields the following coupled set of equations:

$$\begin{aligned} \frac{\partial}{\partial t} q_{l,m}(\mathbf{r}, t) = & -L \sum_{l',m'} \sqrt{\frac{2l'+1}{2l+1}} \left[C_{0,0,0}^{1,l',l} \left(-\frac{1}{\sqrt{2}} (C_{1,m',m}^{1,l',l} + C_{-1,m',m}^{1,l',l}) \frac{\partial}{\partial x} \right. \right. \\ & + \frac{i}{\sqrt{2}} (C_{1,m',m}^{1,l',l} - C_{-1,m',m}^{1,l',l}) \frac{\partial}{\partial y} + C_{0,m',m}^{1,l',l} \frac{\partial}{\partial z} \left. \left. \right) \right] q_{l',m'}(\mathbf{r}, t) \\ & - \frac{1}{2\xi(t)} l(l+1) q_{l,m}(\mathbf{r}, t) \\ & - \sum_{l'',m'',m'''} \sqrt{\frac{(2l''+1)(2l'+1)}{4\pi(2l+1)}} W_{l',m'}(\mathbf{r}) q_{l'',m''}(\mathbf{r}, t) C_{0,0,0}^{l'',l',l} C_{m'',m',m}^{l'',l',l} \end{aligned} \quad (25)$$

with initial conditions

$$q_{0,0}(\mathbf{r}, 0) = \sqrt{4\pi}, \quad q_{l,m}(\mathbf{r}, 0) = 0, \quad \text{otherwise.} \quad (26)$$

A similar equation applies to $q^\dagger(\mathbf{r}, \mathbf{u}, t)$.

2.2. One-dimensional theory

For simple applications of the general theory presented above, we now specialize to situations where the densities vary in only one spatial dimension, which for convenience is chosen to be the z direction. Furthermore, we will restrict analysis to phases that exhibit no azimuthal orientation dependence about the z axis, thereby excluding the possibility of smectic-C phases [17, 21]. Then the only nonzero projections of any angular functions are those with $m = 0$, so that we will subsequently drop the m indices, denoting $\phi_l = \phi_{l,m=0}$, etc. Another consequence is that now all spherical-harmonic expansion coefficients are real. The free energy equation (21) becomes

$$\mathcal{F} = \rho A \sum_l \int dz \left[\frac{4\pi C}{2l+1} d_l \phi_l^2(z) - W_l(z) \phi_l(z) \right] - \ln \frac{Q^n}{n!}, \quad (27)$$

where A is the cross-sectional area of the system in the x and y directions. The mean-field equations (22) and (23) are

$$W_l(z) = \frac{8\pi}{2l+1} d_l C \phi_l(z), \quad (28a)$$

$$\phi_l(z) = \frac{V}{Q} \sum_{l',l''} \int_0^1 dt q_l^\dagger(z, t) q_{l'}(z, t) \sqrt{\frac{(2l''+1)(2l'+1)}{4\pi(2l+1)}} (C_{0,0,0}^{l'',l',l})^2 \quad (28b)$$

with

$$Q = A \sum_l \int dz q_l^\dagger(z, t) q_l(z, t). \quad (29)$$

Finally, the diffusion-like equation (25) becomes

$$\begin{aligned} \frac{\partial}{\partial t} q_l(z, t) = & -L \sum_{l'} \sqrt{\frac{2l'+1}{2l+1}} (C_{0,0,0}^{1,l',l})^2 \frac{\partial}{\partial z} q_{l'}(z, t) - \frac{1}{2\xi(t)} l(l+1) q_l(z, t) \\ & - \sum_{l'',l'''} \sqrt{\frac{(2l''+1)(2l'+1)}{4\pi(2l+1)}} (C_{0,0,0}^{l'',l',l})^2 W_{l'}(z) q_{l''}(z, t) \end{aligned} \quad (30)$$

with initial conditions

$$q_0(z, 0) = \sqrt{4\pi}, \quad q_l(z, 0) = 0, \quad l > 0. \quad (31)$$

In the following, we shall truncate the interaction expansion (19) after $l = 2$, (equivalent to a ‘Maier–Saupe’ interaction), retaining only the terms with coefficients $d_0 = \frac{\pi}{4}$ and $d_2 = -\frac{5\pi}{32}$.

We shall now briefly discuss the computational methods used in solving the theory. The fields and densities are determined self-consistently according to equations (28a), (28b) and (30) using a fixed-point iteration algorithm with variable mixing parameters for successive iterations. An iteration consists of:

- (a) given the functions $W_l(z)$, solving equation (30) and its counterpart for q_l^\dagger ;
- (b) calculating the set of functions $\phi_l(z)$ from equation (28b);
- (c) obtaining a new set of functions $W_l'(z)$ from equation (28a);
- (d) mixing $W_l'(z)$ and $W_l(z)$ according to a fixed-point algorithm, which yields a new $W_l(z)$ for the next iteration.

Concerning step (a), solutions of the diffusion-like equation (30) were discretized in time and space according to a forward time centred space (FTCS) scheme [27], which is explicit and straightforward to implement. This is a reliable discretization scheme for solving partial differential equations although its error is only first order in the contour discretization dt . For the corresponding diffusion equation in the case of Gaussian chains, a number of more sophisticated schemes, such as Crank–Nicholson and DuFort–Frankel [28], are available to improve on stability and accuracy (the error becomes second order in dt in both cases), and thus to lower the contour resolution needed for a given desired level of accuracy, a key factor in computing times. Due to the coupled nature of equation (30), however, it seems daunting to apply similarly efficient discretization schemes to the wormlike chain model.

Concerning step (d), the fixed-point iteration algorithm used in finding self-consistent solutions of equations (28a) and (28b) is a tried and tested method. Here viable alternatives do exist, however, the first and foremost being Newton–Raphson-type algorithms like Broyden’s method (e.g. [29]). In the present work, we have restricted ourselves to using the fixed-point algorithm, since our primary aim was to develop the framework presented above and illustrate it with only a few, demonstrative results.

In the present work, calculations were performed on a one-dimensional grid with periodic boundary conditions, a spatial discretization of $dz = 0.02$ and a contour discretization of $dt = 1/1500$. The spherical-harmonic expansions of the propagators and densities were truncated after $l = 12$. With these parameters, \mathcal{F}/V can be determined to within a numerical inaccuracy of less than 1%, requiring up to 500 iterations, or 3–4 h on a Pentium II processor. Note that, although the interaction kernel (19) is truncated after $l = 2$, we cannot truncate the propagators at the same value of l , since the coupling in (30) renders these higher-order projections nonzero.

Once equations (28a), (28b) and (30) have been solved self-consistently, the free energy can be rewritten as

$$\mathcal{F} = -4\pi C\rho A \sum_l \frac{d_l}{2l+1} \int dz \phi_l^2(z) - \ln \frac{Q^n}{n!}. \quad (32)$$

For determining coexistence regions of the first-order isotropic–nematic transition, it is necessary to perform double-tangent constructions on curves of the free energy per volume \mathcal{F}/V . Omitting linear terms in C (which yield constants when the derivative $\frac{\partial}{\partial C}$ is taken), we obtain

$$\frac{\mathcal{F}}{V} \propto \frac{\mathcal{F}C}{n} = -4\pi C^2 \left(\frac{A}{V} \right) \sum_l \frac{d_l}{2l+1} \int dz \phi_l^2(z) - C \ln \frac{Q}{V} + C \ln C, \quad (33)$$

where we have used Stirling's approximation for the factorial. In a smectic phase, all projections of the local densities and propagators are taken to be periodic functions of z with period (or layer spacing) d . All integrations over z can then be evaluated as

$$\frac{A}{V} \int dz = \frac{1}{d} \int_0^d dz. \quad (34)$$

The location of the second-order nematic–smectic transition (cf section 3) is determined by the behaviour of the smectic order parameter defined as

$$O_{sm} = \left[\frac{1}{d} \int_0^d dz \left([\sqrt{4\pi} \phi_{rigid,0} - f]^2 + [\sqrt{4\pi} \phi_{flex,0} - (1-f)]^2 \right) \right]^{1/2}. \quad (35)$$

The parameter O_{sm} vanishes in the isotropic and nematic phases, while it is nonzero in the smectic phase. For a ‘perfect’ smectic phase in which the profiles $\sqrt{4\pi} \phi_{rigid,0}$ and $\sqrt{4\pi} \phi_{flex,0}$ have rectangular shapes of widths fd and $(1-f)d$, respectively, O_{sm} has the value $\sqrt{2f(1-f)}$. The equilibrium period is that value of d which minimizes the free energy per volume.

3. Results

The results presented here apply to a fluid of polymers with $\xi_{rigid} = 10$, and $\xi_{flex} = 0.1$. These values more or less represent the feasible bounds on ξ for performing numerical calculations. To begin with, we shall examine a system with $f = 2/3$.

Figure 1 shows the rigid and flexible density profiles (i.e. zeroth-order projections $\phi_{\beta,l=0}(z)$, $\beta \in \{\text{rigid}, \text{flex}\}$) as well as the total density profile $\phi_0(z)$ in a smectic configuration at $C = 20$, just above the nematic–smectic transition. We see a clearly defined region of predominantly rigid chain segments and a less pronounced region where the flexible parts are dominant. The individual density variations are nearly pure sine functions, as expected close to a second-order transition. The total density in this lamellar structure exhibits maxima in the rigid regions and minima in the flexible regions. This indicates that the rigid segments pack more efficiently than flexible ones due to their greater susceptibility to local orientational alignment. The non-constant value of the total density $\phi_0(z)$ also reflects the fact that we have not imposed an incompressibility constraint, as discussed in section 2.

More insight can be gained from the orientational projections of the densities, $\phi_{\beta,l}(z)$. Here we express these in terms of the z -dependent order parameters defined as, for each degree l ,

$$\bar{P}_{l,\beta}(z) = \frac{1}{\sqrt{2l+1}} \frac{\phi_{\beta,l}(z)}{\phi_{\beta,0}(z)}, \quad (36)$$

equivalent to the average of the l th Legendre polynomial $P_l(\cos \theta)$ per segment of species β , where θ is the angle between a segment axis and the z axis. The lowest-order functions $\bar{P}_{1,\beta}(z)$ and $\bar{P}_{2,\beta}(z)$ corresponding to the configuration of figure 1 are shown in figures 2 and 3. The second-order distribution $\bar{P}_{2,\beta}$ characterizes the overall degree of orientational order of species β , while $\bar{P}_{1,\beta}$ indicates the average spatial direction in which segments β are oriented. The behaviour of the functions $\bar{P}_{1,\beta}(z)$ shows that both the rigid and flexible regions are divided in the middle into domains of positive and negative orientation along z , in the manner of a bilayer. We see that both $\bar{P}_{2,rigid}$ and $\bar{P}_{2,flex}$ exhibit maxima (minima) in the regions of high (low) rod density (cf figure 1). The minimum in the flexible coil distribution $\bar{P}_{2,flex}$ is more pronounced, while its maximal region is a slightly modulated plateau within the domain of high rigid density, suggesting that coil segments are oriented by interactions with neighbouring rigid segments. Overall, the coils exhibit a much weaker degree of orientational ordering than the rods.

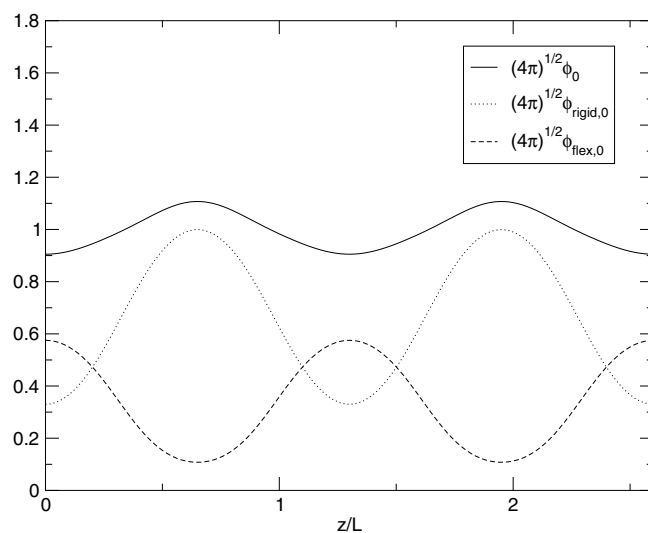


Figure 1. Density profiles of a smectic configuration with $f = 2/3$, $\xi_{rigid} = 10$, $\xi_{flex} = 0.1$, $C = 20$ and period $1.3L$. The full, dotted and broken curves correspond to $\sqrt{4\pi}\phi_0$, $\sqrt{4\pi}\phi_{rigid,0}$, and $\sqrt{4\pi}\phi_{flex,0}$, respectively.

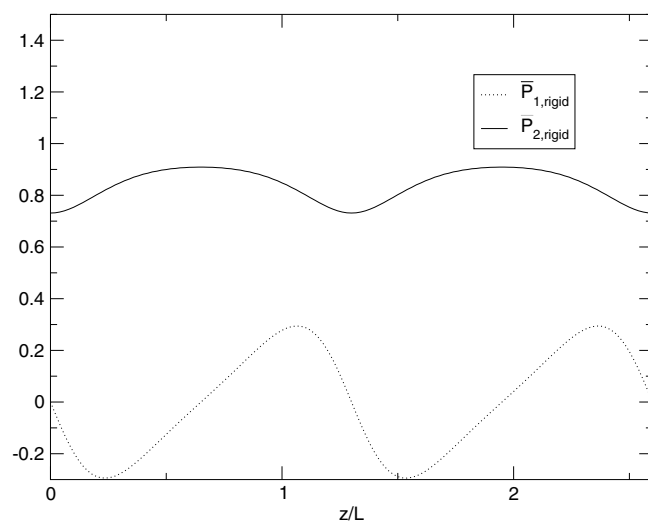


Figure 2. Orientational order parameters $\bar{P}_{1,rigid}$ (dotted curve) and $\bar{P}_{2,rigid}$ (full curve) for the same case as in figure 1.

The configuration shown in figures 1–3 has an optimal period (i.e. yielding the minimum free energy per volume) of $d = 1.30L$ for the chosen parameters $f = 2/3$ and $C = 20$. Keeping the same f but increasing C to 30 results in a decrease of the optimal period to $d = 1.24$. This is accompanied by stronger segregation of the rod and coil regions and less purely sinusoidal behaviour of the densities, as shown in figure 4. The corresponding orientational order parameters are given in figures 5 and 6, and are qualitatively similar to those for $C = 20$. We have found that the optimal periods range from $1.1L$ for $f = 0.3$

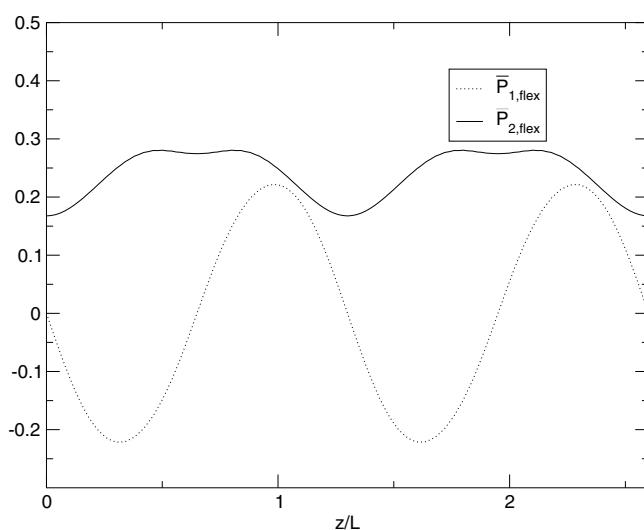


Figure 3. Order parameters $\bar{P}_{1,flex}$ (dotted curve) and $\bar{P}_{2,flex}$ (full curve) for the same case as in figure 1.

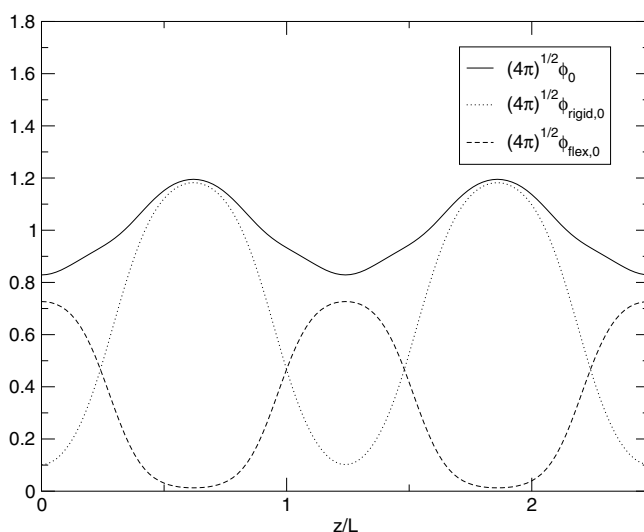


Figure 4. Density profiles as in figure 1 but for $f = 2/3$, $C = 30$ and period $1.24L$.

to $1.3L$ for $f = 0.75$ for values of C close to the $N-A_d$ transition. Smectic phases with values of f outside this interval could not be examined due to numerical difficulties. Attempts to generate solutions corresponding to monolayer smectic structures having $d \leq L$ always converged to a uniform (isotropic or nematic) phase.

Figure 7 shows the phase diagram in the $C-f$ plane for rod-coil polymers with $\xi_{rigid} = 10$ and $\xi_{flex} = 0.1$. At low mean densities C , the steric interactions do not suffice to generate an ordered phase: the system is isotropic. Upon increasing C , we encounter a first-order isotropic-nematic (I-N) transition. The two branches delineating the coexistence region in the diagram were determined by constructing tangents to the \mathcal{F}/V graphs for the isotropic and

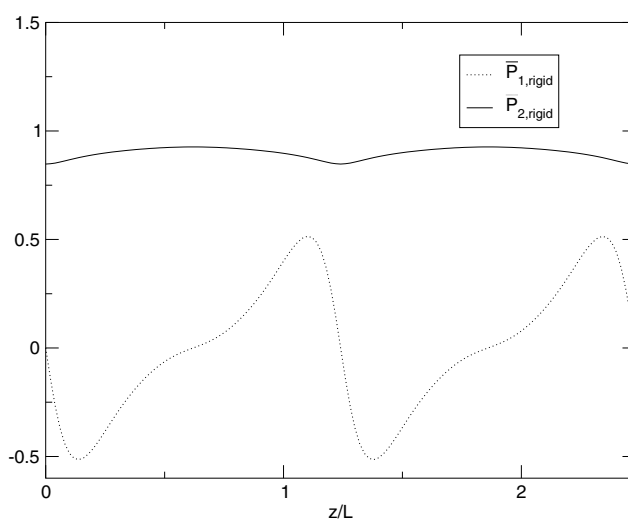


Figure 5. Orientational order parameters of rigid segments for the same case as in figure 4.

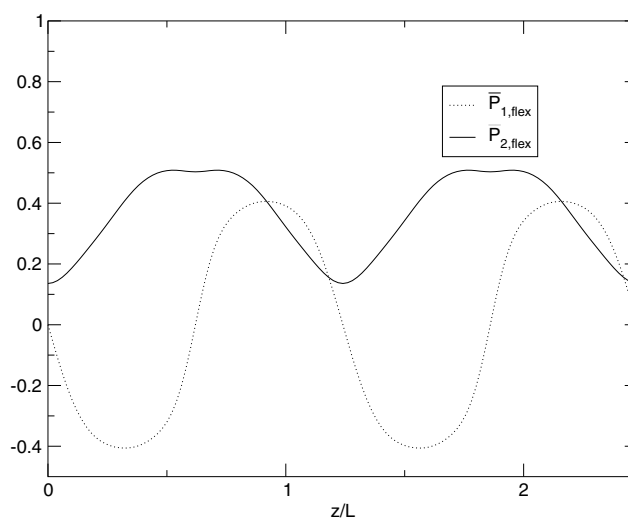


Figure 6. Orientational order parameters of flexible segments for the same case as in figure 4.

nematic solutions with a spline interpolation, which amounts to calculating the values of C at equal chemical potentials and pressures. The lower f , the higher is the value of C at which the I–N transition occurs: this transition is driven primarily by the tendency of the rigid-rod segments to align and thus requires higher densities if the proportion of the rods is lowered. For $f = 1$ we can compare our data with that of Chen [13], who uses the full kernel (19) and obtains an isotropic density of $C_{iso} = 4.18$ and a nematic density of $C_{nem} = 5.33$. If we calculate this transition retaining the kernel up to $l = 12$, we obtain good agreement: $C_{iso} = 4.16$ and $C_{nem} = 5.29$. With the truncated kernel ($l \leq 2$) used in the majority of this work, the coexistence region becomes narrower: $C_{iso} = 4.89$ and $C_{nem} = 5.35$.

A second transition, from the nematic to the smectic (A_d) phase, occurs at higher values of C . This transition is second order within numerical uncertainties, as is indicated by the

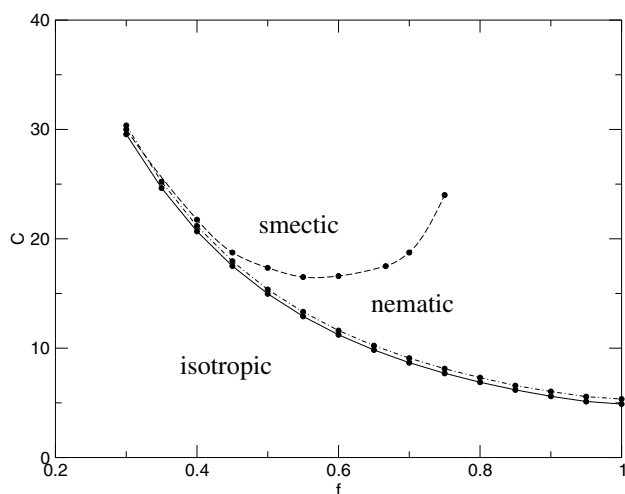


Figure 7. Phase diagram for rod-coil copolymers with $\xi_{rigid} = 10$, $\xi_{flex} = 0.1$. The isotropic and nematic phases are separated by a narrow coexistence region bounded by the full and chain curves. The boundary between smectic and nematic phases is second order, indicated by the broken curve.

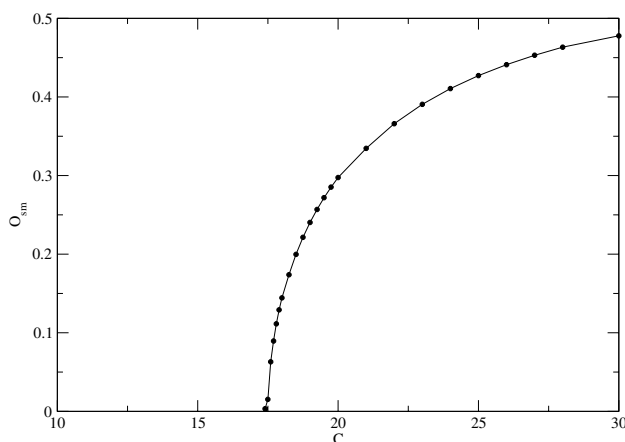


Figure 8. Smectic order parameter versus C for $f = 2/3$.

behaviour of the smectic order parameter O_{sm} , equation (35). Figure 8 shows that O_{sm} starts to grow from zero at a well-defined critical value of the density C . There is a minimum of the $N-A_d$ transition density at roughly $f = 0.55$. On moving toward both lower and higher values of f , the critical values of C increase sharply until numerical difficulties prevent us from extending the graph further. Obviously, a well-balanced proportion of rod-like versus coil-like segments facilitates forming a smectic phase: the former stabilize the rod-dominated portion of the density profile (the nematic microdomain, as it were) and the latter, the coil-dominated portion. Deviations from the optimal f to higher values of f decrease the entropic advantage of the coils, which has to be compensated for by an increased density. Lower values of f , on the other hand, destabilize the nematic microdomain ordering of the rods. This is why, for even lower values of f , the I-N and $N-A_d$ phase boundaries approach each other until intersecting at $f = 0.32$. Below this value of f , the I-N transition is preempted by a first-order $I-A_d$ transition. For

$f = 0.3$, we find a coexistence region between $C_{iso} = 29.3$ and $C_{smec} = 31.4$. Unfortunately, numerical problems prevented us from examining even lower values of f : it thus remains an open question by how much the $I-A_d$ transition deviates from the preempted I–N transition.

4. Summary and conclusions

We have presented a SCFT for semiflexible copolymers in a general three-dimensional, as well as a one-dimensional, form without azimuthal orientational dependence. Using this framework, numerical calculations have been performed to investigate the occurrence of a smectic-A phase in systems of rod–coil copolymers where the two parts of each molecule differ only in their rigidities.

A phase diagram was established for $\xi_{rigid} = 10$ and $\xi_{flex} = 0.1$, which correspond to very stiff rods and very flexible coils. At low reduced density C , an isotropic phase is present, which becomes nematic for larger values of C via a first-order transition. At even larger values of C , a partial bilayer smectic-A phase forms, whose period increases with increasing rod fraction f . The latter effect, while small in the examined parameter range, indicates that the coils can overlap with other coil segments as well as with the rods, resulting in interdigitation of the layers. This feature is also suggested by the rather diffuse, sinusoidal variation of the local density profiles $\phi_{\beta,0}$. The shape of the smectic phase boundary in figure 7, exhibiting a minimum mean density C near a rod fraction $f = 0.55$, is plausible and consistent with experimental deductions [21] (see also [30]). Preliminary calculations indicate that lowering the rod rigidity ξ_{rigid} shifts all transitions to higher densities C .

In the present work, only anisotropic excluded-volume interactions between chain segments, assumed to be the same for the rigid and flexible portions of each molecule, are taken into account. To generate smectic phases, we have shown that it is sufficient to distinguish rigid and flexible parts of a polymer by means of their rigidities or reduced persistence lengths ξ , and thus have demonstrated that lamellar ordering is a purely entropic phenomenon. This is consistent with the findings of computer simulations [18, 20–23] and a density-functional treatment [24] of diblock models employing only anisotropic repulsive intermolecular forces. In contrast, the smectic ordering found in the SCFT treatments of [16, 17] is driven primarily by *isotropic* Flory–Huggins interactions between unlike chain segments, which may well be present in more realistic models. Unlike here, the latter works predicted the formation of both monolayer and bilayer smectic phases, as well as strong segregation between rigid and flexible domains, which we attribute both to the quite different nature of the interactions adopted and to the allowance of local compressibility in the present theory: as conjectured in [17], compressibility effects ‘could dramatically stabilize the bilayer phase’.

Due to our use of the Onsager second-virial approximation for treating repulsive interactions between polymers, the present theory is valid only for dilute solutions in the limits that the volume fraction $\rho V_{mol} \rightarrow 0$ and $L/D \rightarrow \infty$ such that $C \equiv \rho DL^2$ remains finite and non-zero [15]. Here $V_{mol} \propto LD^2$ is the molecular volume. In previous studies employing the Onsager approximation [13–15], these limits have been applicable only to the isotropic–nematic phase transition. The phase diagram of figure 7 shows that smectic ordering induced by differing rigidities can occur under the same limiting conditions. Figure 7 also indicates that the values of C at the nematic–smectic transition increase sharply with increasing f , that is, approaching the limit of homogeneous and fairly rigid chains. This is consistent with studies showing the existence of smectic phases in such fluids at non-zero volume fraction [31–34]. In this limit the Onsager theory should still be qualitatively valid, but the spatially local form adopted in equation (4) should be generalized to a non-local interaction in order to generate smectic phases in fluids of homogeneous wormlike chains [33].

Future extensions of the theory presented here will attempt to account for the non-local interactions mentioned in the preceding paragraph as well as for smectic-C phases, crystallization of the rods and non-lamellar morphologies, all of which are expected to occur at larger values of the number density ρ and more extreme values of the rod fraction f . To examine larger densities, higher-virial corrections to the free energy should be taken into account, for example, by the approach of Parsons [15, 35].

Acknowledgments

We thank F Schmid and M Matsen for fruitful discussions. This work was supported through grants from the Deutsche Forschungsgemeinschaft (DFG) and the Natural Sciences and Engineering Research Council (Canada) (NSERC).

References

- [1] de Gennes P G and Prost J 1993 *The Physics of Liquid Crystals* 2nd edn (Oxford: Clarendon)
- [2] Gray G W 1979 *The Molecular Physics of Liquid Crystals* ed G R Luckhurst and G W Gray (New York: Academic)
- [3] Stegemeyer H 1994 *Liquid Crystals* (Berlin: Springer)
- [4] Bates F S and Fredrickson G H 1990 *Annu. Rev. Phys. Chem.* **41** 525
- [5] Helfand E 1975 *J. Chem. Phys.* **62** 999
- [6] Hong K M and Noolandi J 1981 *Macromolecules* **14** 727
- [7] Scheutjens J M H M and Fleer G J 1979 *J. Chem. Phys.* **83** 1619
- [8] Schmid F 1998 *J. Phys.: Condens. Matter* **10** 8105
- [9] Matsen M W 2002 *J. Phys.: Condens. Matter* **14** R21
- [10] Saito N, Takahashi K and Yunoki Y 1967 *J. Phys. Soc. Japan* **22** 219
- [11] Morse D A and Fredrickson G H 1994 *Phys. Rev. Lett.* **73** 3235
- [12] Matsen M W 1996 *J. Chem. Phys.* **104** 7758
- [13] Netz R R and Schick M 1996 *Phys. Rev. Lett.* **77** 302
- [14] Chen Z Y 1993 *Macromolecules* **26** 3419
- [15] Cui S-M, Akcakir O and Chen Z Y 1995 *Phys. Rev. E* **51** 4548
- [16] Semenov A N and Khokhlov A R 1988 *Sov. Phys.-Usp.* **31** 988
- [17] Semenov A N and Vasilenko S V 1986 *Sov. Phys.-JETP* **63** 70
- [18] Matsen M W and Barrett C 1998 *J. Chem. Phys.* **109** 4108
- [19] Nicklas K, Bopp P and Brickmann J 1994 *J. Chem. Phys.* **101** 3157
- [20] Affouard F, Kröger M and Hess S 1996 *Phys. Rev. E* **54** 5178
- [21] Mazars M, Levesque D and Weis J-J 1997 *J. Chem. Phys.* **106** 6107
- [22] Casey A and Harrowell P 1999 *J. Chem. Phys.* **110** 12183
- [23] van Duijneveldt J S, Gil-Villegas A, Jackson G and Allen M P 2000 *J. Chem. Phys.* **112** 9092
- [24] McBride C, Vega C and MacDowell L G 2001 *Phys. Rev. E* **64** 011703
- [25] Holyst R 1990 *Phys. Rev. A* **42** 3438
- [26] Chen J T, Thomas E L, Ober C K and Mao G-P 1995 *Macromolecules* **28** 1688
- [27] Chen J T, Thomas E L, Ober C K and Mao G-P 1996 *Science* **273** 343
- [28] Gray C G and Gubbins K E 1984 *Theory of Molecular Fluids: vol 1. Fundamentals* (Oxford: Clarendon)
- [29] Press W H, Flannery B P, Teukolsky S A and Vetterling W T 1986 *Numerical Recipes* (Cambridge: Cambridge University Press)
- [30] Mitchell A R and Griffiths D F 1980 *The Finite Difference Method in Partial Differential Equations* (Chichester: Wiley)
- [31] Eyert V 1996 *J. Comput. Phys.* **124** 271
- [32] Müller M and Schick M 1996 *Macromolecules* **29** 8900
- [33] Sear R P and Jackson G 1995 *Phys. Rev. E* **52** 3881
- [34] Bladon P and Frenkel D 1996 *J. Phys.: Condens. Matter* **8** 9445
- [35] van der Schoot P 1996 *J. Physique II* **6** 1557
- [36] Dogic Z and Fraden S 1997 *Phys. Rev. Lett.* **78** 2417
- [37] Parsons J D 1979 *Phys. Rev. A* **19** 1225